Technical Report Documentation Page

1. Report No. FHWA/TX-09/0-5549-2	2. Government Accession No.	3. Recipient's Catalog No.
4. Title and Subtitle Horizontal Cracking Mechanism in CRCP		5. Report Date February 2009, Revised June 2009 6. Performing Organization Code
7. Author(s) Seongcheol Choi, Moon Won, Elias Sudoi, Seifollah Nasrazadani		8. Performing Organization Report No. 0-5549-2
9. Performing Organization Name and Address Center for Transportation Research The University of Texas at Austin 3208 Red River, Suite 200, Austin, TX 78705-2650 Center for Multidisciplinary Research Texas Tech University 10th and Akron, Lubbock, TX 79409 Engineering Technology Department University of North Texas 3940 North Elm St. Suite F-115, Denton, TX 76207		10. Work Unit No. (TRAIS) 11. Contract or Grant No. 0-5549
12. Sponsoring Agency Name and Address Texas Department of Transportation Research and Technology Implementation Office P.O. Box 5080 Austin, TX 78763-5080		13. Type of Report and Period Covered Technical Report 09/2006-02/2009 14. Sponsoring Agency Code

15. Supplementary Notes
Project performed in cooperation with the Texas Department of Transportation and the Federal Highway Administration.

16. Abstract

The purpose of this study is to identify the mechanism of horizontal cracking in continuously reinforced concrete pavement (CRCP). To this end, a numerical model to predict the risk of horizontal cracking in CRCP was developed. Material properties and steel design were considered in the numerical analysis and their effects on the risk of horizontal cracking were investigated. Based on numerical analysis results, laboratory testing was also conducted in order to simulate the horizontal cracking in transverse crack interface in CRCP. A horizontal cracking frame was developed and the mechanism of horizontal cracking was experimentally investigated. Longitudinal steel plays a significant role in developing horizontal cracks in CRCP. Significant stress of concrete develops near longitudinal steel because of steel restraint. It indicates that the horizontal crack perpendicular to maximum stress of concrete can occur near the steel. The horizontal cracks initiate from the transverse crack interface and propagate along the longitudinal steel. The effects of rebar temperature at the concrete placement and the water-to-cement ratio on the concrete rebar bond strength were also investigated experimentally.

17. Key Words Horizontal cracking, CRCP, concrete, longitudinal steel, bond strength, corrosion, rebar temperature, water-to-cement ratio	18. Distribution Statement No restrictions. This document is available to the public through the National Technical Information Service, Springfield, Virginia 22161; www.ntis.gov.

19. Security Classif. (of report) Unclassified	20. Security Classif. (of this page) Unclassified	21. No. of pages 52	22. Price

Form DOT F 1700.7 (8-72) Reproduction of completed page authorized

Horizontal Cracking Mechanism in CRCP

Seongcheol Choi
Moon Won
Elias Sudoi
Seifollah Nasrazadani

CTR Technical Report:	0-5549-2
Report Date:	February 2009
Project:	0-5549
Project Title:	Horizontal Cracking in Concrete Pavement
Sponsoring Agency:	Texas Department of Transportation
Performing Agencies:	Center for Transportation Research at The University of Texas at Austin The Center for Multidisciplinary Research in Transportation at Texas Tech University Engineering Technology Department at the University of North Texas

Project performed in cooperation with the Texas Department of Transportation and the Federal Highway Administration.

Center for Transportation Research
The University of Texas at Austin
3208 Red River
Austin, TX 78705

www.utexas.edu/research/ctr

Disclaimers

Author's Disclaimer: The contents of this report reflect the views of the authors, who are responsible for the facts and the accuracy of the data presented herein. The contents do not necessarily reflect the official view or policies of the Federal Highway Administration or the Texas Department of Transportation (TxDOT). This report does not constitute a standard, specification, or regulation.

Patent Disclaimer: There was no invention or discovery conceived or first actually reduced to practice in the course of or under this contract, including any art, method, process, machine manufacture, design or composition of matter, or any new useful improvement thereof, or any variety of plant, which is or may be patentable under the patent laws of the United States of America or any foreign country.

Engineering Disclaimer

NOT INTENDED FOR CONSTRUCTION, BIDDING, OR PERMIT PURPOSES.

Project Engineer: Moon Won
Professional Engineer License State and Number: Texas No. 76918
P. E. Designation: Research Supervisor

Acknowledgments

The authors would thank TxDOT for its financial support for the project.

Table of Contents

List of Figures

List of Tables

Chapter 1. Introduction

1.1 Research background

Recently, it has been reported that different types of cracking have taken place in continuously reinforced concrete pavement (CRCP) that has had structural improvement, i.e., thicker slabs, stabilized bases, and tied concrete shoulders. These cracks, which cannot be explained by traditional theories related to punchout and spalling, are normally associated with horizontal cracking at approximately mid-depth of the slab. It was also observed that horizontal cracks took place at early ages before the pavement was open to traffic. These findings strongly indicate that horizontal cracks are not due to structural deficiencies of CRCP. Rather, concrete material properties, environmental conditions during and right after concrete placement, and longitudinal steel placement layouts might play a significant role in the development of horizontal cracking. This distress type has not been well recognized by researchers and practitioners until recently. A research study is necessary to understand the mechanism of this type of distress.

1.2 Objective and scope of the research

Although the performance of CRCP has been excellent, some CRCP sections have been rehabilitated before their design lives were reached. Distresses such as punchout and spalling lead to the deterioration of CRCP. Recently, it has been found during full-depth repair of CRCP that a different form of punchout, which is associated with horizontal cracking at the depth of longitudinal steel, occurred in CRCP. This type of cracking may eventually cause distress in CRCP, which should be minimized. The purpose of this study is to identify the mechanism of horizontal cracking in CRCP.

In order to identify the mechanism of horizontal cracking, a numerical model was developed to represent the behavior of CRCP under environmental loading. The stress of concrete at the depth of steel where the horizontal crack generally occurs was predicted through the numerical method. Concrete material and steel design were considered in the numerical analysis and their effects on the risk of horizontal cracking were predicted. Based on the numerical analysis results, laboratory testing was also conducted to investigate the mechanism of horizontal cracking. The horizontal cracking frame was developed to simulate the behavior of CRCP under environmental loading. The occurrence of transverse and horizontal cracks was experimentally measured in the test. The risk of horizontal cracking for different concrete materials was compared.

Water-to-cement (w/c) ratios and their influence on concrete bond strength were also investigated. Rebar temperatures at the concrete placement stage were studied in order to simulate cold, normal, and hot days, mimicking the actual field conditions in which CRCP construction takes place. This allowed the investigation of the effect of environmental condition on rebar concrete bond strength.

1.3 Report organization

This chapter was prepared by the Center for Transportation Research (CTR) at The University of Texas at Austin and the Center for Multidisciplinary Research in Transportation at Texas Tech University (TechMRT).

Chapter 2 summarizes the findings of numerical analysis of the mechanism of horizontal cracking, which was performed by CTR and TechMRT.

Chapter 3 describes laboratory evaluation of the horizontal cracking mechanism using a horizontal cracking frame. This was conducted by CTR and TechMRT.

Chapter 4 presents the effects of rebar temperature and water-to-cement ratio on the bond strength of concrete rebar, which was prepared by University of North Texas (UNT).

Chapter 5 summarizes the horizontal cracking mechanism data presented in Chapters 2 and 3 by CTR and TechMRT and the bond strength test results presented in Chapter 4 by UNT.

Chapter 2. Identification of Horizontal Cracking Mechanism

2.1 Numerical model

Cracking in concrete takes place when the stress exceeds the strength. In order to identify the appropriate horizontal cracking mechanism, it is required to accurately predict the distribution of strain and stress fields in concrete at the depth of reinforcement. The state of stress in concrete near the reinforcement can be analyzed through a two-dimensional finite element method. Environmental loadings due to changes in temperature and moisture were considered in the numerical analysis. Fig. 2.1 show the finite element model for prediction of horizontal cracking in CRCP. If CRCP is subject to environmental loading, the CRCP behavior can be assumed to be symmetric with respect to the center of the two adjacent transverse cracks. Therefore, one-half of the slab was considered in the numerical model. The concrete slab was modeled using two-dimensional plane elements. The longitudinal steel bars were discretized using frame elements. The boundary conditions of the finite element model should be defined to obtain the correct prediction of structural behavior under environmental loadings. At the transverse crack, it is assumed that no restraint was applied to the concrete. Longitudinal and rotational displacement was fixed at the point of the reinforced bar at the transverse crack interface. At the center for slab, a vertical degree of freedom existed and longitudinal and rotational displacements were restrained.

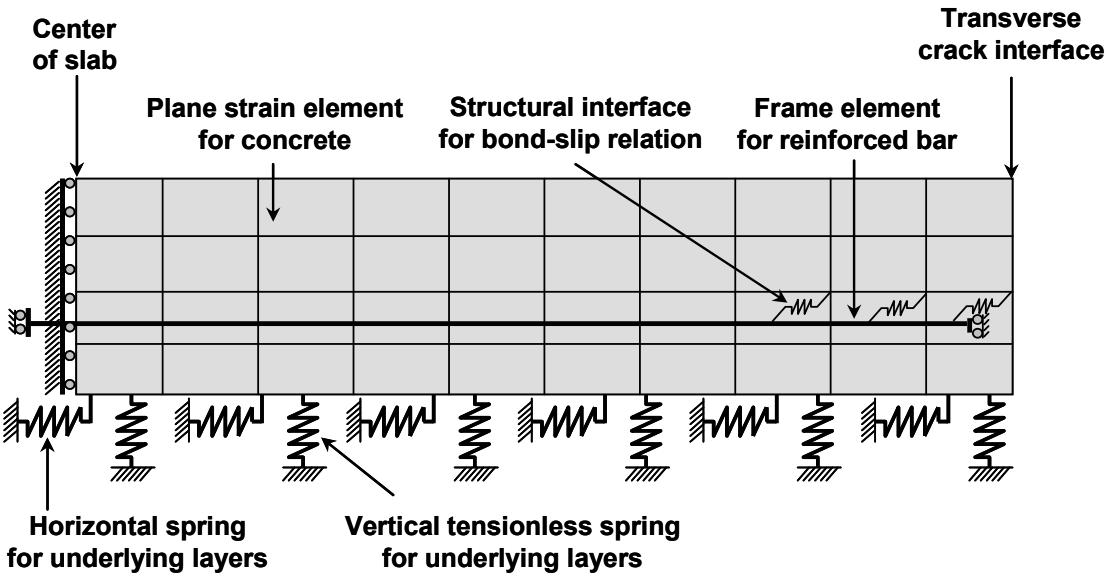

Figure 2.1: Finite element model for prediction of horizontal cracking in CRCP

The bond-slip relation between concrete and longitudinal steel bars was considered through the interface element with horizontal springs. The frictional slip that occurs at the interface between the bottom of the concrete slab and the base layer was considered through the horizontal spring element. A vertical tensionless spring was used to properly consider the curling effect. The vertical tensionless spring stiffness per unit area in this study was 0.1 MPa/mm (400 psi/in). Figure 2.2-(a) indicates the frictional stress-slip relationship between concrete and

subbase (Kim et al., 1997). Horizontal stiffness for the interface between the concrete and subbase was assumed to be 0.04 MPa/mm (150 psi/in). In order to predict the strain of tie bar, the bond stress-slip relationship in Figure 2.2-(b) was used (Kim et al., 2000).

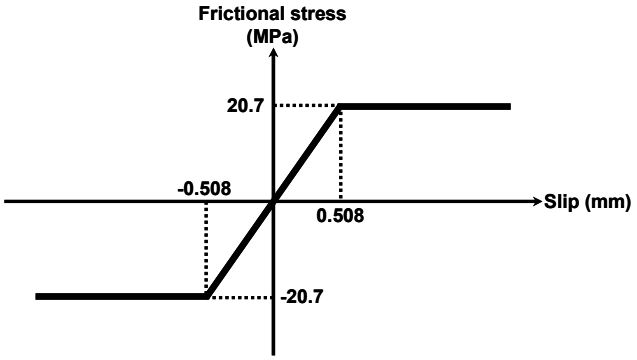

(a) Frictional stress-slip relationship between concrete and subbase
(1 mm = 0.0394 in; 1 MPa = 145 psi)

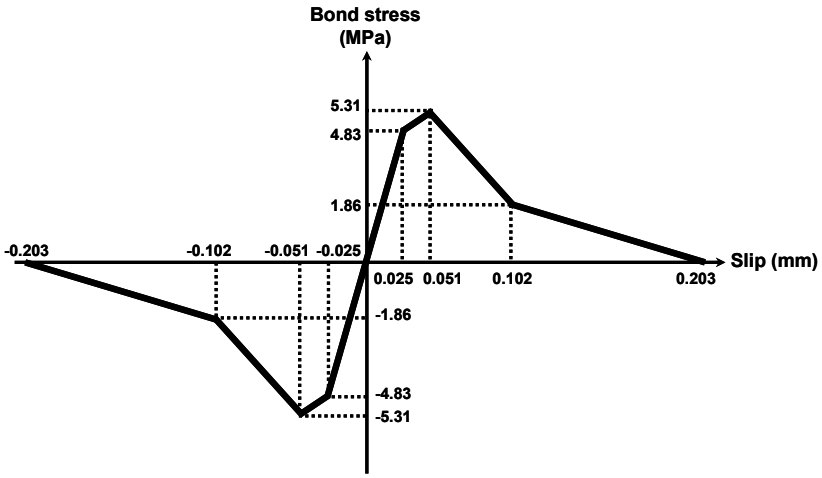

(b) bond stress-slip relationship between concrete and tie bar
(1 mm = 0.0394 in; 1 MPa = 145 psi)

Figure 2.2: Interface stress-slip relationships used in the numerical analysis

Table 2.1 represents the default input for numerical analysis. In the numerical analysis, the spacing of the transverse crack was assumed to be 10 ft with a pavement thickness of 14 in. The temperature difference of 30˚F between the top and bottom of the slab was applied as an environmental loading. The variation of coefficient of thermal expansion (CTE) and elastic modulus of concrete was analysis factors. As different coarse aggregates can cause changes in the CTE and elastic modulus of concrete, their effects were analyzed in the numerical analysis. Longitudinal steel design was also an analysis parameter. One-mat and two-mat placement of longitudinal steel was modeled and the corresponding stress was compared. Additionally, the effects of bond-slip condition and the depth of transverse crack on the risk of horizontal cracking were investigated in the numerical analysis.

Table 2.1: Default input in the numerical analysis

Transverse crack spacing	10 ft
Pavement thickness	14 in
Amount of steel	0.6% with #6 bar
Temperature difference	30°F between top and bottom
Coefficient of thermal expansion	4×10^{-6}/°F
Elastic modulus of concrete	4×10^{6} psi
Elastic modulus of steel	29×10^{6} psi

2.2 Effects of various factors on the risk of horizontal cracking in CRCP

2.2.1 Coefficient of thermal expansion (CTE)

In order to investigate the effect of concrete's CTE on the risk of horizontal cracking, two different CTEs for concrete, 4×10^{-6}/°F and 6×10^{-6}/°F, were used and the stress of concrete near steel was compared. Fig. 2.3-(a) shows the stress distribution in the numerical model between the transverse cracks shown in Fig. 2.1. Maximum principal stress of 4.26 MPa (618 psi) occurred at the depth of steel at the transverse crack with an assumed CTE of 4×10^{-6}/°F. If this principal stress exceeds the strength of concrete, the crack will develop in the direction perpendicular to the principal stress. Fig. 2.3-(b) shows the directional vector of principal stress in concrete. At the depth of steel, the principal stress was at the maximum and the direction was nearly vertical with a slight upward or downward direction. Therefore, the horizontal cracking can occur near the reinforced steel.

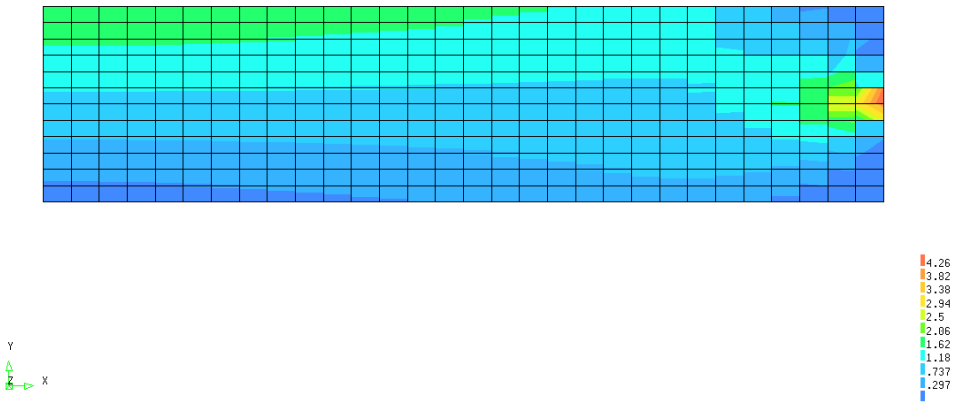

(a) Distribution of principal stress in CRCP with CTE= 4×10^{-6}/°F (1MPa=145 psi)

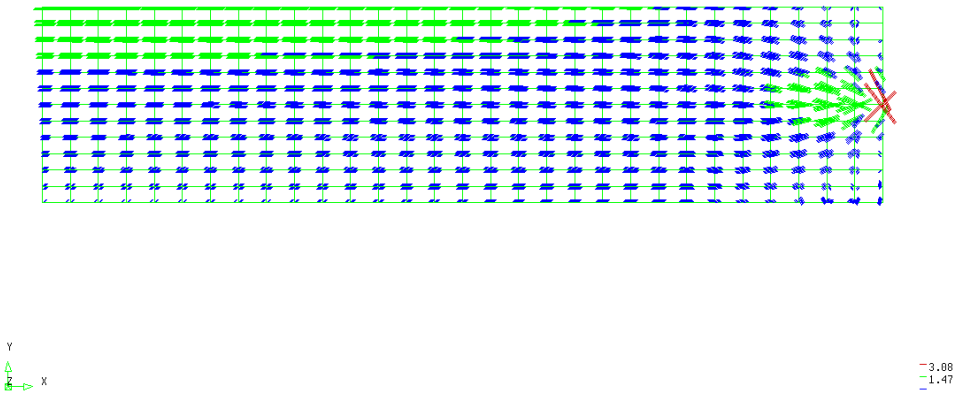

(b) Directional vector of principal stress in CRCP with CTE= 4×10^{-6}/°F (1MPa=145 psi)

Figure 2.3: Distribution and direction vector of concrete principal stress with CTE= 4×10^{-6}/°F

Fig. 2.4 shows the distribution and directional vector of principal stress in CRCP when a CTE of 6×10^{-6}/°F was assumed. The distribution and directional vector of principal stress in Fig. 2.4 were very similar to that in Fig. 2.3. However, the maximum principal stress was 5.98 MPa (867 psi) at the depth of steel, which was 1.72 MPa (249 psi) greater than that of concrete with a CTE of 4×10^{-6}/°F. This indicates the effect of concrete's CTE on the risk of horizontal cracking. It is expected that a higher CTE causes more volume changes that will be restrained by reinforced steels, leading to higher stress development in concrete near the reinforced steel. It explains why there are more horizontal cracks in the concrete with higher CTE such as concrete containing siliceous river gravel (SRG) coarse aggregate than in the concrete with lime stone (LS) coarse concrete.

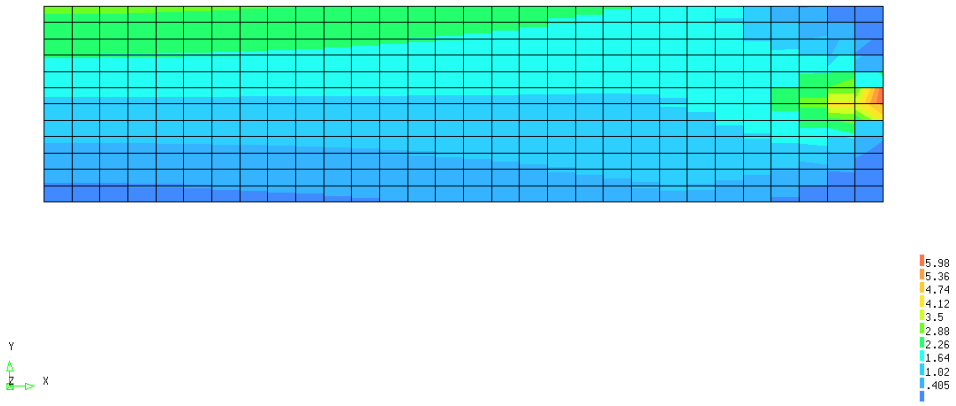

(a) Distribution of principal stress in CRCP with CTE= 6×10^{-6}/°F (1MPa=145 psi)

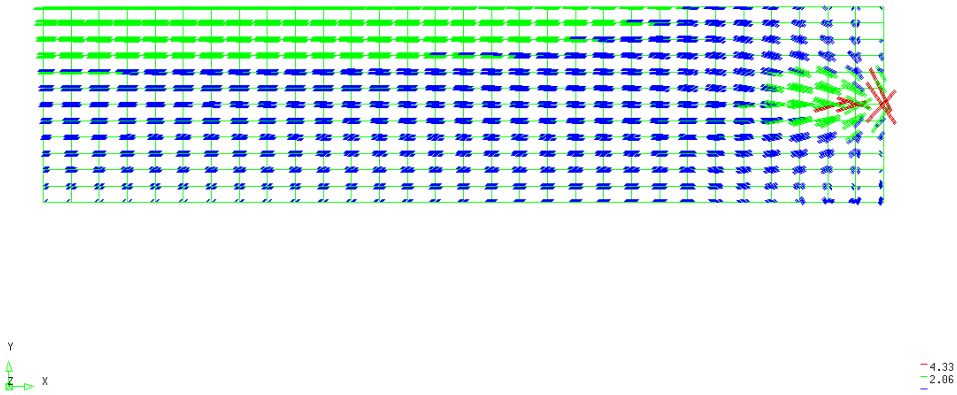

(b) Directional vector of principal stress in CRCP with CTE= 6×10^{-6}/°F (1MPa=145 psi)

Figure 2.4: Distribution and direction vector of concrete principal stress with CTE= 6×10^{-6}/°F

2.2.2 Elastic modulus

In order to investigate the effect of concrete elastic modulus on the risk of horizontal cracking in CRCP, two different values of elastic modulus of concrete—4×10^{6} psi and 6×10^{6} psi, which are typical values of concrete with LS coarse aggregate and SRG coarse aggregate, respectively— were selected in the numerical analysis. It was assumed that all the material properties except elastic modulus were the same even though different elastic modulus may be correlated to different material properties such as CTE. CTE was assumed to be 4×10^{-6}/°F in the numerical analysis. Fig. 2.5 shows the effect of concrete elastic modulus on the distribution of principal stress in CRCP. As expected, the maximum principal stress occurred at the depth of reinforced steel. The CRCP with concrete elastic modulus of 4×10^{6} psi (27.6 MPa) and 6×10^{6} psi (41.4 MPa) resulted in 618 psi (4.26 MPa) and 770 psi (5.31 MPa), respectively. Higher elastic modulus increased the stress in concrete near the steel. It explains the effect of concrete elastic modulus on the risk of horizontal cracking in CRCP. There are more horizontal cracks in the concrete with SRG coarse aggregate than in concrete with LS coarse aggregate.

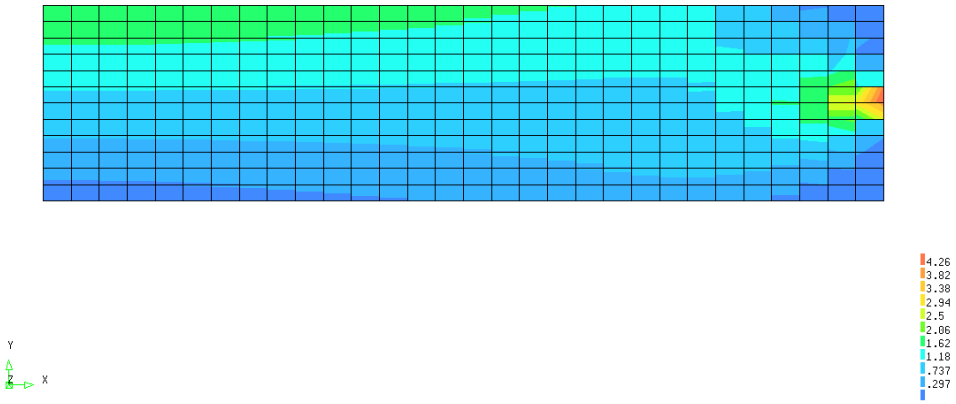

(a) Distribution of principal stress in CRCP with elastic modulus = 4×10^6 psi (27.6 MPa) (1MPa=145 psi)

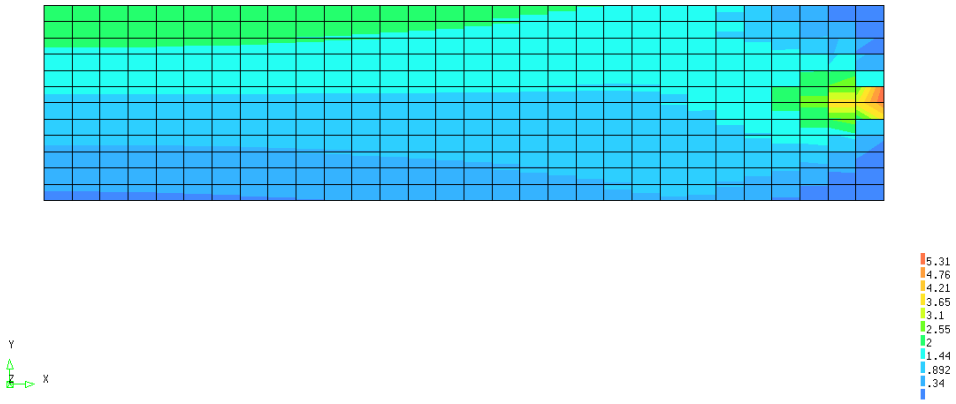

(b) Distribution of principal stress in CRCP with elastic modulus = 6×10^6 psi (41.4 MPa) (1MPa=145 psi)

Figure 2.5: Effect of elastic modulus on the risk of horizontal cracking in CRCP

2.2.3 Longitudinal steel design

In order to avoid horizontal cracking in CRCP, TxDOT uses both one-mat and two-mat placement of longitudinal bars in CRCP. The different placement of longitudinal bars was considered in the numerical analysis to investigate its effect on the risk of horizontal cracking. CTE and elastic modulus of concrete were 4×10^{-6}/°F and 4×10^6 psi (27.6 MPa), respectively. Fig. 2.6-(a) shows the distribution of principal stress with one-mat placement of longitudinal steel at mid-depth (7 in.). The steel ratio of 0.6% with #6 bar was placed at mid-depth and the spacing was 6 in. The maximum stress was 618 psi (4.26 MPa) at the steel depth. Fig. 2.6-(b) depicts the distribution of principal stress with two-mat placement of longitudinal steel. Two-mat longitudinal steels were placed at the depths of 4.7 in. and 9.4 in. with 12 in. spacing, respectively. The maximum stress of concrete—457 psi (3.15 MPa)—occurred at 4.7 in. depth. This result indicates that the risk of horizontal cracking in CRCP can be reduced through two-

mat placement of longitudinal steel. Two-mat placement of longitudinal steel split up the restraint for the volume change of concrete and thus the stress was relieved.

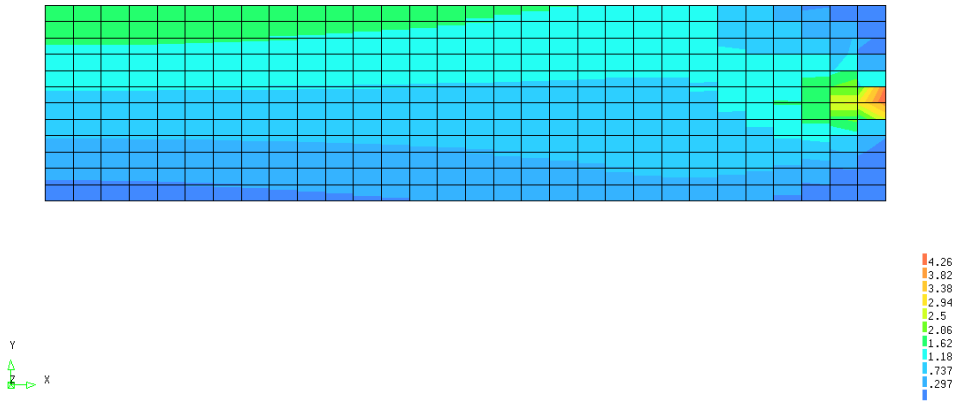

(a) Distribution of principal stress in CRCP with one-mat placement of longitudinal steel (1MPa=145 psi)

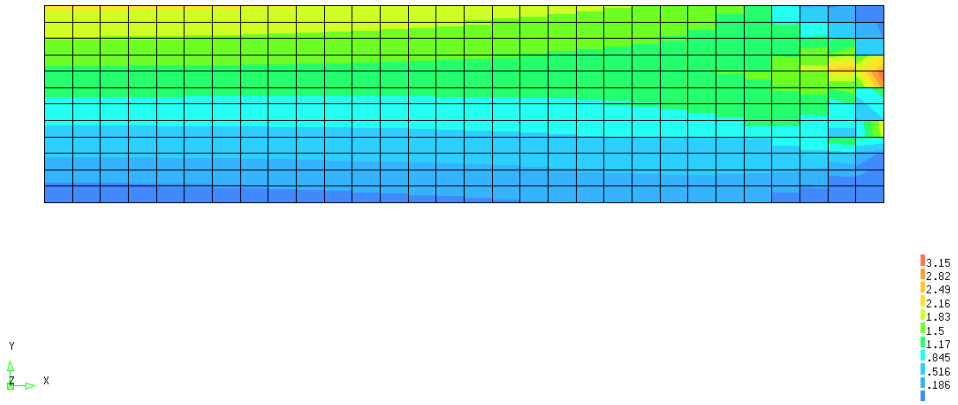

(b) Distribution of principal stress in CRCP with two-mat placement of longitudinal steel (1MPa=145 psi)

Figure 2.6: Effect of longitudinal steel design on the risk of horizontal cracking in CRCP

Fig. 2.7 shows the comparison of principal stress when one-mat longitudinal steel is placed at different depths. The maximum stress of 626 psi (4.32 MPa) occurred at the steel depth of 3.5 in., which was slightly greater than stress in 7.0 in. depth (617 psi). When CRCP is cast in the field, its surface is exposed to environmental conditions such as temperature and relative humidity. More volume changes occur at the surface region than core region. More restraint leads to the increase of concrete stress at steel depth. This indicates that the risk of horizontal cracking may be increased when the steel is placed closely to the exposed surface.

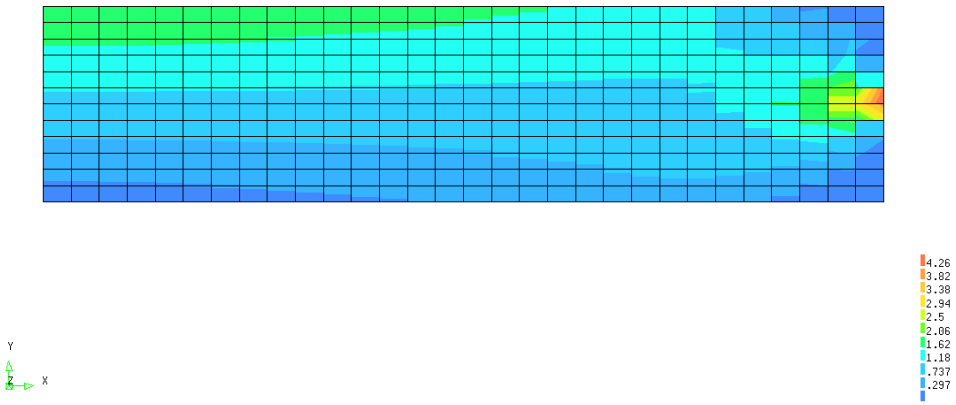

(a) Principal stress with one-mat placement of longitudinal steel at mid depth 7 in. (1MPa=145 psi)

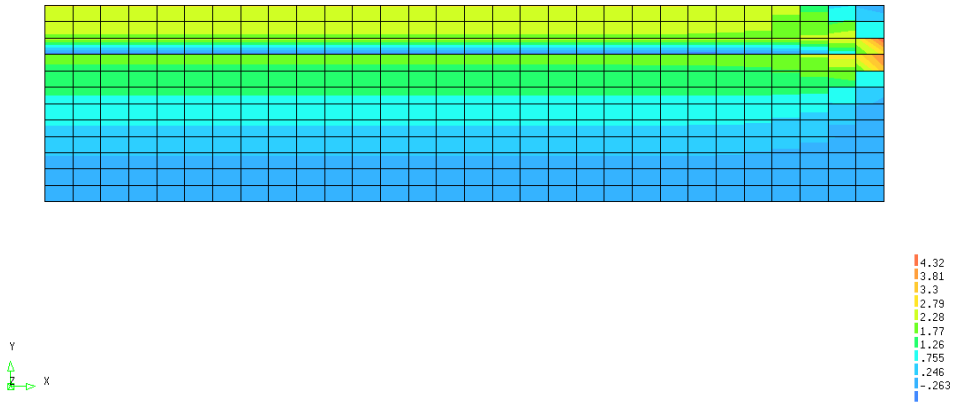

(b) Principal stress with one-mat placement of longitudinal steel at mid depth 3.5 in. (1MPa=145 psi)

Figure 2.7: Effect of longitudinal steel depth on the risk of horizontal cracking in CRCP

2.2.4 Bond-slip relation

The volume changes due to the variations of temperature and moisture are restrained by the reinforced steel and this restraint results in the maximum principal stress at the depth of steel. Therefore, the reinforced steel plays a significant role in stress development in concrete at transverse crack interface. The effect of bond-slip on the risk of horizontal cracking was investigated. Fig. 2.8 shows the stress development, in which the bond-slip relation was employed, as shown in Fig. 2.2-(b). The maximum stress was 617 psi (4.26 MPa). When full bond relation, i.e., no slip, is assumed, concrete stress increased significantly. The maximum stress of concrete was 1305 psi (9.0 MPa), which was almost twice as much as stress with bond-slip relation. Under the full bond condition, the concrete volume changes were restrained further and this caused the increase of concrete stress.

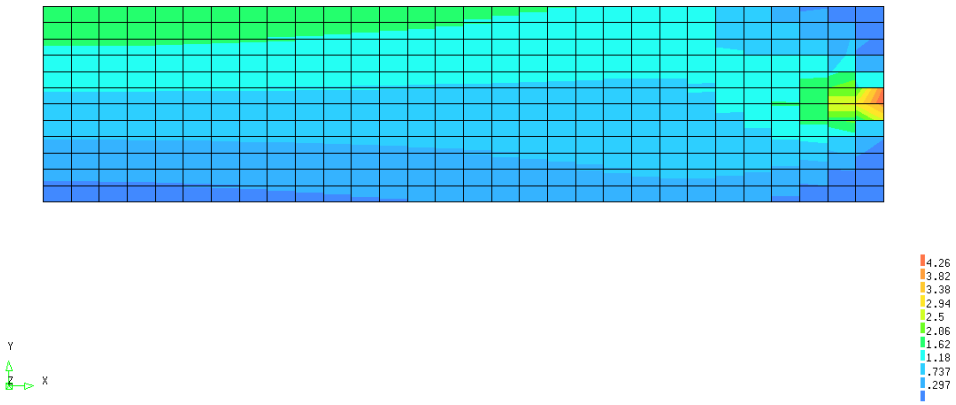

(a) Principal stress in CRCP considering bond-slip relation (1MPa=145 psi)

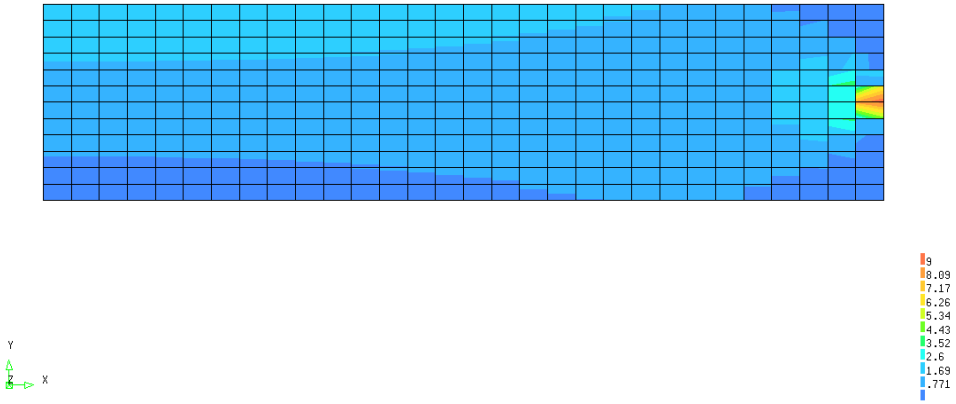

(b) Principal stress in CRCP assuming full bond (1MPa=145 psi)

Figure 2.8: Effect of bond-slip relation on the risk of horizontal cracking in CRCP

2.2.5 Partial-depth and full-depth transverse crack

The transverse cracking of CRCP is generally caused by the environmental loading at early ages. Cracking may initiate at the surface of slab and propagate to the full-depth or partial-depth of slab. The risk of horizontal cracks in CRCP with full-depth and partial-depth transverse crack was investigated. Fig. 2.9 shows the analysis results with the assumption of full-depth (14 in.) and partial-depth (7 in.) transverse crack. While the maximum stress was 617 psi (4.26 MPa) in the slab with full-depth transverse crack, the maximum was 973 psi (6.71 MPa) in the slab with partial-depth transverse crack. This is because the movement of concrete was solely restrained by the steel. The stress of concrete near the reinforced steel was concentrated further and thus the principal stress increased. It indicates that the risk of horizontal cracking may increase for the CRCP with partial-depth transverse crack.

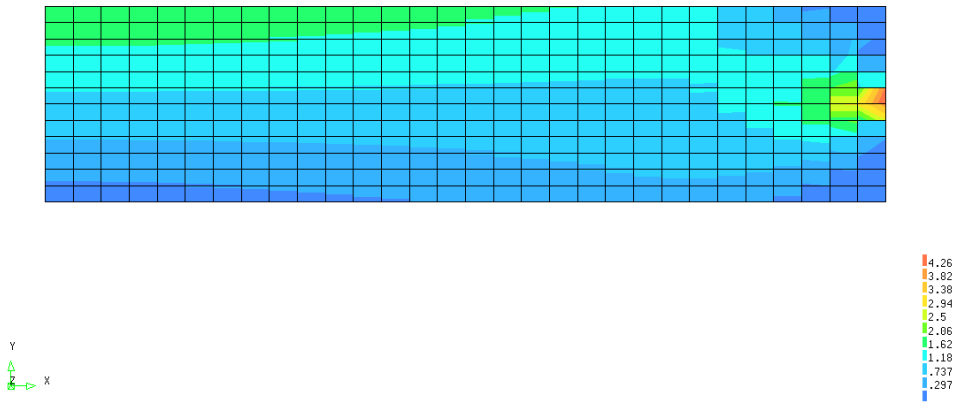

(a) Principal stress in CRCP with full-depth crack
(1MPa=145 psi)

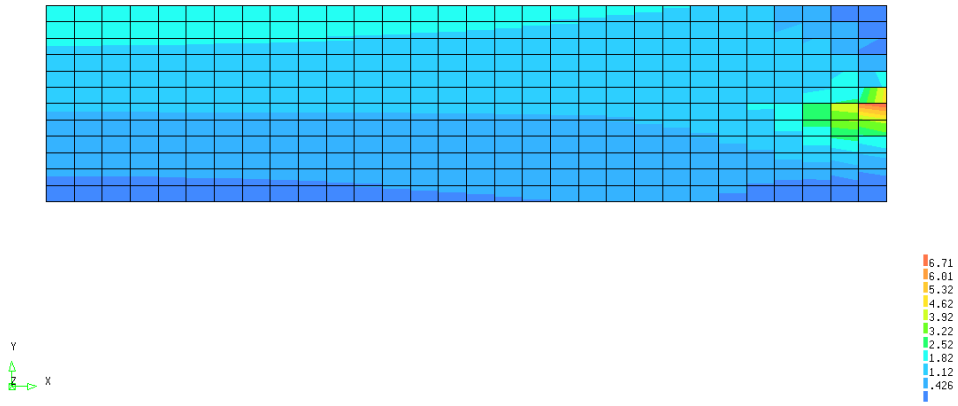

(b) Principal stress in CRCP with partial-depth crack
(1MPa=145 psi)

Figure 2.9: Risk of horizontal cracking in CRCP with full-depth and partial-depth transverse crack

2.3 Summary

Horizontal cracking in CRCP and its causes were investigated through the numerical analysis. A numerical model of CRCP was developed using finite element discretization to predict the stress distribution of concrete. The findings from the numerical analysis are summarized as follows.

1. Horizontal cracks initiate and propagate from the transverse crack interface at the depth of longitudinal steel. Environmental loading, such as variations in temperature and moisture, plays a major role in the development of horizontal cracks in CRCP. The longitudinal steel provides the restraint condition for the movement of concrete and this restraint results in stress of concrete.
2. The stress in concrete is the maximum at the depth of steel in transverse crack interface. The direction of this stress is almost vertical with a slight upward or

downward direction. If the maximum stress exceeds the strength of concrete, the crack will develop in the horizontal direction.

3. The effect of various material properties on the risk of horizontal cracking in CRCP was investigated in the numerical analysis. The results are as follow.

   - **Coefficient of thermal expansion:** a higher CTE of concrete increases the concrete stress at the depth of steel. As CTE becomes higher, more volume change will occur, which will be restrained by the longitudinal steel. It agrees with the field survey results that there are more horizontal cracks in the concrete with SRG than LS.
   - **Elastic modulus:** the stress of concrete increased with high elastic modulus of concrete. This also agrees with the field study that there are more horizontal cracks in SRG concrete than in LS concrete.
   - **Longitudinal steel design:** compared to one-mat placement of longitudinal bar, two-mat placement reduced the maximum stress of concrete. The restraint action by longitudinal steel was split up and thus corresponding stress of concrete diminished.
   - **Bond-slip relation:** the assumption of full-bond between concrete and reinforced steel provided more restraint of concrete movement and thus caused higher stress than bond-slip relation.
   - **Depth of transverse crack:** a higher stress of concrete was concentrated at the depth of steel in a slab with partial-depth cracking; the risk of horizontal cracking may increase.

4. In order to reduce the risk of horizontal cracking in CRCP, the following is recommended:

   - The type of coarse aggregate should be considered in order to produce low CTE and elastic modulus of concrete;
   - Two-mat placement of longitudinal steel should be used for thicker CRCP.

Chapter 3. Laboratory Evaluation of Horizontal Cracking Mechanism

3.1 Horizontal cracking frame

In order to identify horizontal cracking mechanism, a cracking frame at the J.J. Pickle Research Center at the University of Texas was slightly modified. This modified device will be called Horizontal Cracking Frame (HCF) hereinafter. The cracking frame was originally developed primarily for the evaluation of the thermal cracking potential of plain concrete without longitudinal steel (Springenschmid, 1998). As shown in Fig. 3.1, the original cracking frame consists of a frame with two cross heads and two massive steel frame bars. Each steel frame bar, made of invar to minimize displacement due to temperature variations, has a diameter of 100 mm (about 4 in.). The water circulated through the pipe in the thermally insulated formwork can be adjusted so that the temperature of specimen in the frame can match target concrete temperature.

A primary modification to the original cracking frame is to use reinforcing steel in the middle of the concrete specimen as such shown in Fig. 3.2. Fig. 3.3 illustrates the detailed diagram of HCF. It is shown that a rebar is inserted in the middle of the concrete, simulating the longitudinal steel (#6 bar) in CRCP.

Figure 3.1: Cracking frame

Figure 3.2: Horizontal cracking frame

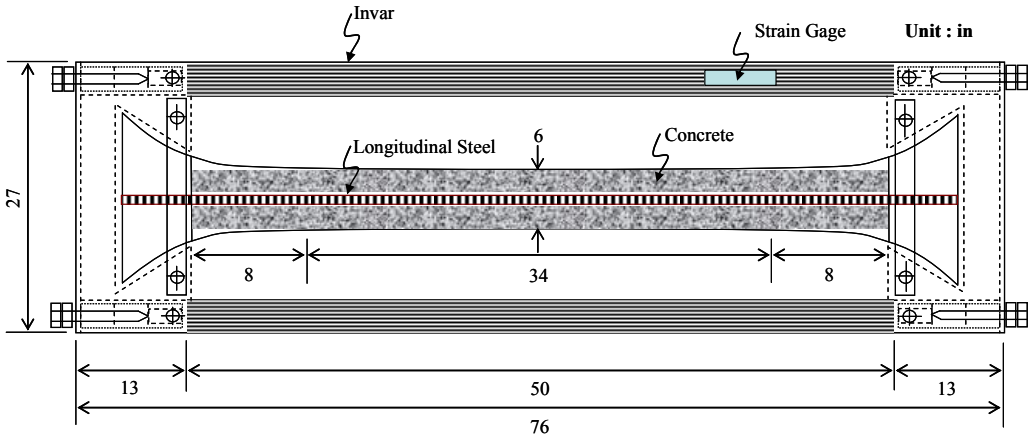

(a) Plan view of HCF

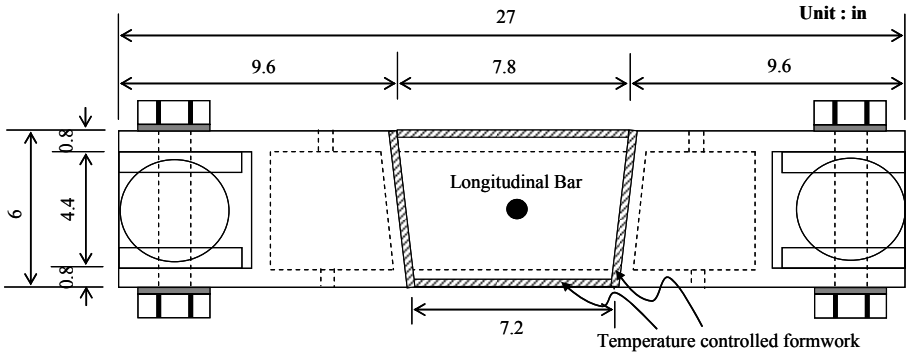

(b) Cross view of HCF

Figure 3.3: Details of HCF

3.2 Experimental procedure

3.2.1 Material

Two different types of aggregate—i.e., siliceous rive gravel (SRG) and lime stone (LS)—were used in the mixture to compare the effect of CTE and elastic modulus on the risk of the horizontal cracking. Table 3.1 summarizes the mixture proportion in the test.

Table 3.1: Mixture proportion in testing

	Unit	Mix-1
Cement type I/II	lb/yd^3	470
Water	lb/yd^3	211.5
Coarse Aggregate	lb/yd^3	1942
Fine Aggregate	lb/yd^3	1245
Air entraining agent	$fl\ oz/yd^3$	1.2
Superplasticizer	$fl\ oz/yd^3$	14.1
Water-to-cementitious ratio	-	0.45
Air content	%	4.5

Table 3.2 summarizes the mechanical properties of material used in the testing. As expected, the concrete with SRG aggregate had higher compressive strength and elastic modulus at 28 days.

Table 3.2: Mechanical properties of material in testing

	28-day compressive strength [psi]	28-day elastic modulus [10^6 psi]
Concrete with LS aggregate	5409	4.88
Concrete with SRG aggregate	6714	6.01

3.2.2 Concrete strain measurement

Vibrating wire strain gages (VWSGs) were installed to measure the temperature and strain in concrete specimen. Three EM-5 VWSGs were installed in the longitudinal direction at different depth (1 in., 3 in., and 5 in.) from the top surface. These gages measured the longitudinal strain and it is expected that the strain will jump if the transverse crack occurs in the specimen. In order to induce the crack at the center of specimen, two acrylic plates (6 in. height, 1 in. width, and 1/2 in. thickness) were placed at the center of specimen. Two EM-2 VWSGs were also installed vertically at the mid-depth (3 in.) in the center of specimen. These EM-2 gages will experience the sudden increase of strain when the horizontal crack occurs. Fig. 3.4 shows the installed VWSG in horizontal cracking frame.

(a) Plan view of installed VWSGs

(b) Installed VWSGs

Figure 3.4: Installed VWSGs to measure transverse and horizontal cracks

3.3 Test results

3.3.1 Temperature in limestone concrete

Fig. 3.5 shows the measured temperature history of LS concrete. At early stages, the temperature was heated up to 110°F and maintained at 105°F until concrete age of three days. During this period, concrete was being hardened. In order to simulate the transverse cracking, the specimen was cooled down to 70°F. Because the volume change of the specimen was restrained

by the frame, the tensile stress would build up in the specimen during cooling stages. The transverse crack is expected when the developed tensile stress exceeds the strength.

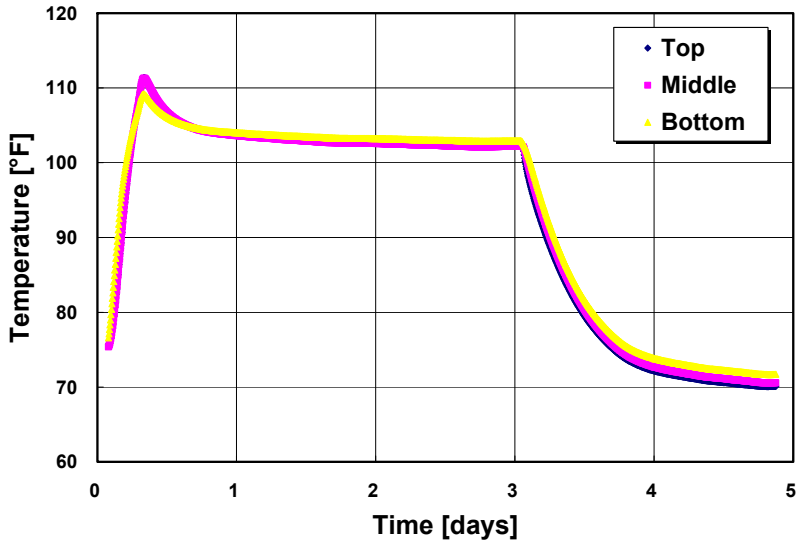

Figure 3.5: Measured temperature histories in limestone concrete specimen

3.3.2 Strain in limestone concrete

Fig. 3.6 shows the measured strains of VWSGs installed in longitudinal and vertical directions in limestone concrete specimen. The measured strains show very similar variation to temperature changes. The strains initially increased and were maintained constantly as temperature changed. As the temperature started to drop, the strains also decreased. At the age of 3.4 days, the strain suddenly jumped up and it is considered that this sudden increase was due to the crack occurrence.

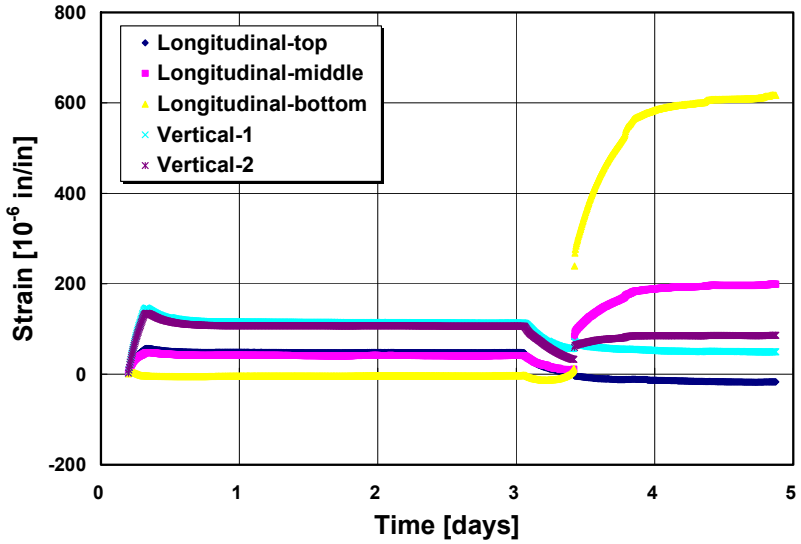

Figure 3.6: Measured strain histories in limestone concrete specimen

The variations of strain due to crack occurrence were magnified and shown in Fig. 3.7. There were significant increases at longitudinal strain [see Fig. 3.7-(a)]. As shown in Fig. 3.7-(b), the vertical strain of 30×10^{-6} in./in. also suddenly increased. Therefore, horizontal cracking occurred in the specimen.

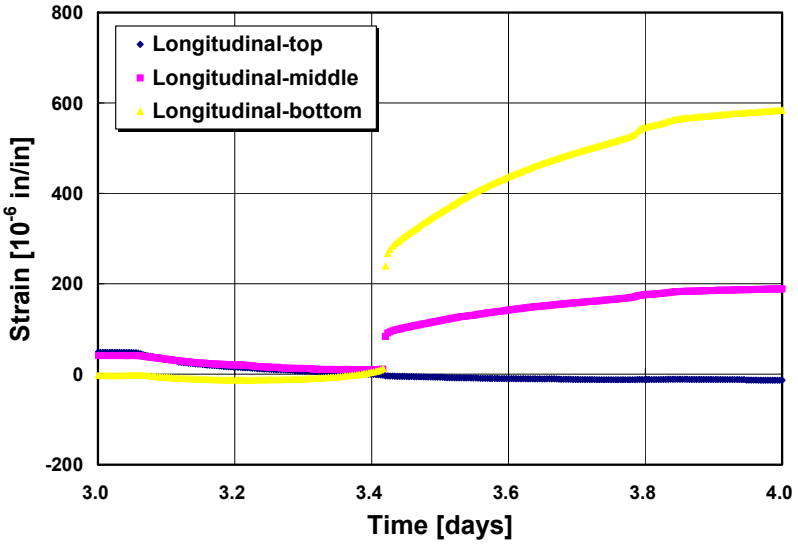

(a) Variation of longitudinal strain due to crack occurrence

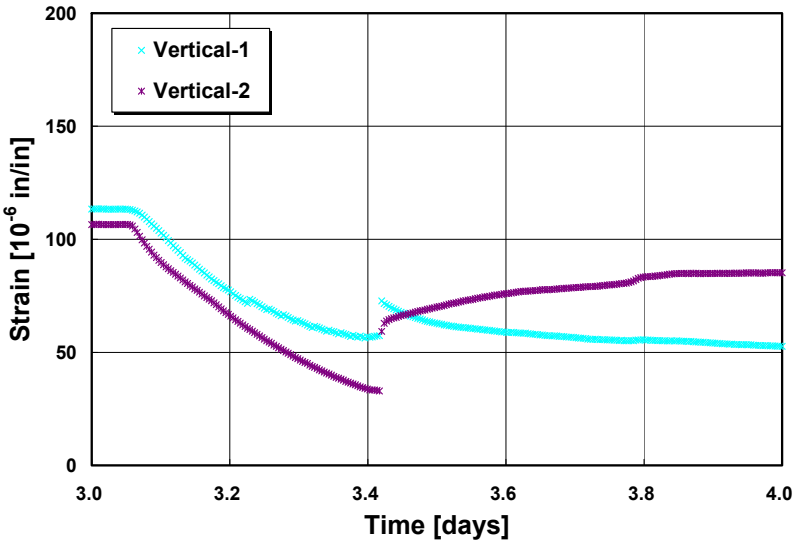

(b) Variation of vertical strain due to crack occurrence

Figure 3.7: Variation of strain due to crack occurrence in limestone concrete specimen

3.3.3 Temperature in SRG concrete

Fig. 3.8 shows the measured temperature history of SRG concrete specimen. The temperature was heated up to 110°F at early stages and cooled down to 75°F in order to induce the transverse crack.

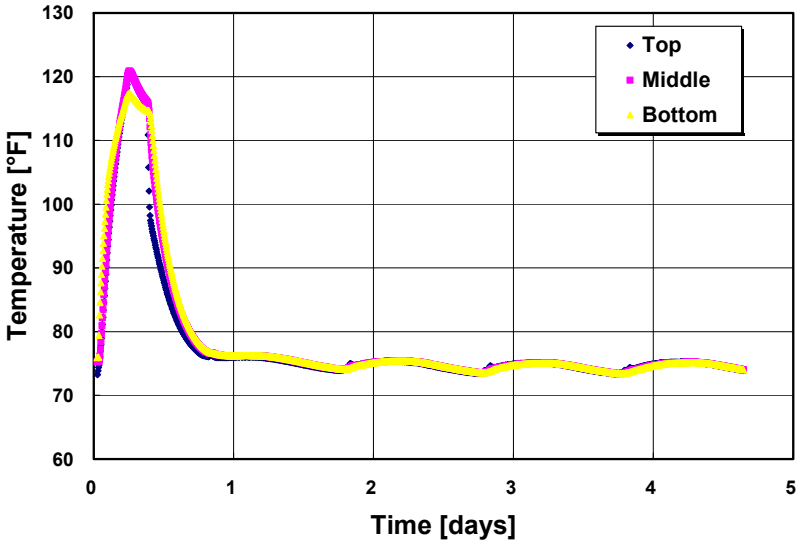

Figure 3.8: Measured temperature histories in SRG concrete

3.3.4 Strain in SRG concrete

Fig. 3.9 shows the measured strain histories of VWSGs installed in longitudinal and vertical directions in SRG concrete specimen. Before the occurrence of crack, the variation of strain was very similar to temperature changes. The strains initially increased and then decreased as the temperature changed. The sudden increases of longitudinal and vertical strain occurred at about 0.4 day and this was due to the occurrence of transverse and horizontal cracks.

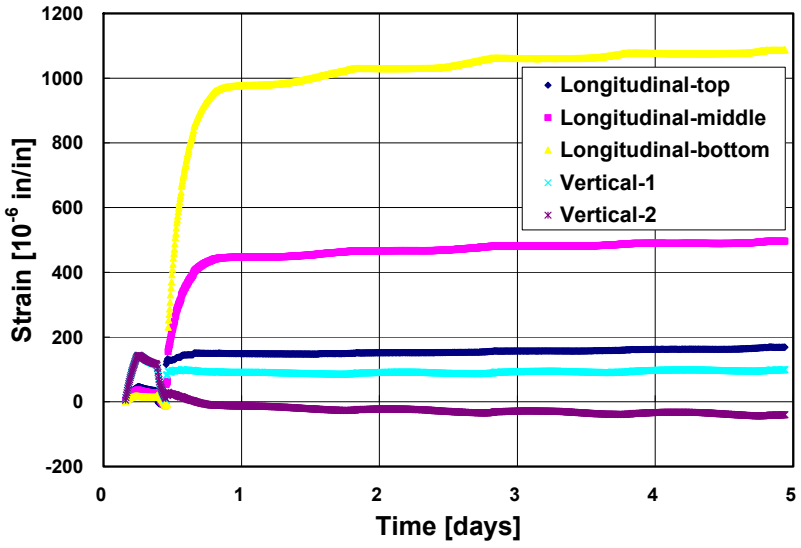

Figure 3.9: Measured strain histories in SRG concrete specimen

The variations of strain due to crack occurrence were magnified and shown in Fig. 3.10. The longitudinal strain increased significantly at 0.45 day. This is because the transverse crack occurred at this age. The sudden increases also took place in measured vertical strain at mid-depth, in which the longitudinal steel was placed. This increase indicates that the horizontal cracking occurred in the SRG concrete near the longitudinal steel. The sudden jump of vertical strain of 75×10^{-6} in./in. was caused by the horizontal cracking.

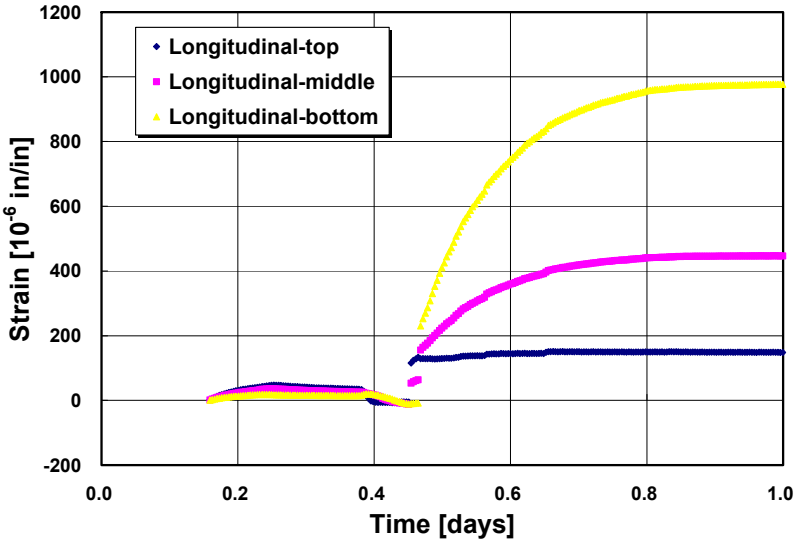

(a) Variation of longitudinal strain due to crack occurrence

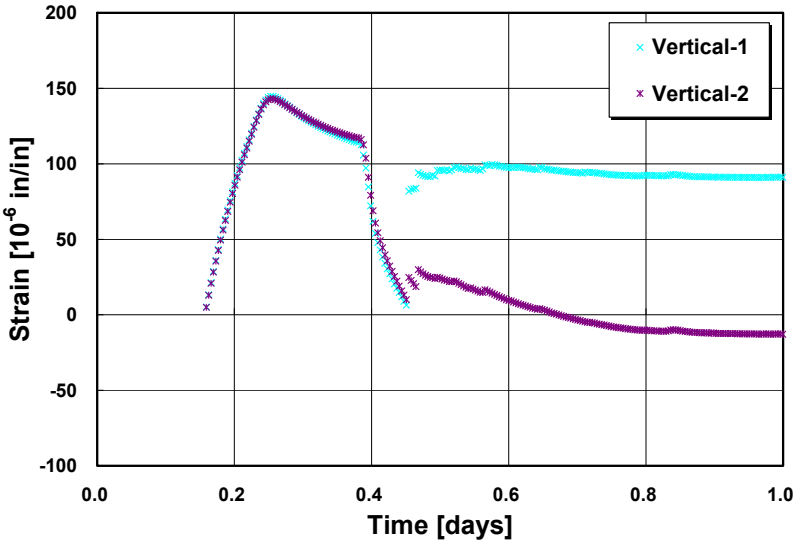

(b) Variation of vertical strain due to crack occurrence

Figure 3.10: Variation of strain due to crack occurrence in SRG concrete specimen

3.4 Discussion of test results

The test results suggest that transverse cracks can develop when the volume changes of concrete due to temperature drop are restrained. Longitudinal strain suddenly increased when the transverse crack occurred. The strain gage installed vertically at mid-depth near longitudinal steel also experienced the sudden increase of measured strain, which indicates the occurrence of horizontal cracking. The amount of strain increase due to horizontal cracking was greater in SRG concrete than in LS concrete. This is because the CTE and elastic modulus of SRG concrete is larger than those of LS concrete. This result agreed with numerical analysis in the previous chapter. It is shown from laboratory testing that horizontal cracking takes place near the steel when transverse crack occur during temperature cooling stage. SRG concrete is more likely to induce the horizontal cracking than LS concrete, an outcome that agrees with the numerical analysis results.

Chapter 4. Factors Affecting Horizontal Cracking in CRCP

4.1 Introduction

This chapter presents the results of an experimental investigation to identify the significant microscale factors influencing horizontal cracking in continuously reinforced concrete pavements (CRCP). An analysis was conducted of the microstructure, morphological characteristics of the interfacial transition zone (ITZ) and the observations on the cracking using the environmental scanning electron microscope (ESEM). Characterization of corrosion products on the surface of the oxidized rebar samples using Fourier Transform Infrared Spectroscopy (FTIR) and Energy Dispersive x-ray Spectroscopy (EDS) was also performed. The effects of the water-to-cement ratio (w/c) and rebar temperature on rebar-concrete bonding were assessed and results showed a significant influence of these parameters on the rebar-concrete bond strength. The 28-day shear strength measurements showed an increase in rebar-concrete bond strength as the w/c was reduced from 0.50 to 0.40. There was a reduction in the peak pullout strength as the temperature increased from 14^{o}F to 252^{o}F for the corroded and non-corroded rebar experiments. FTIR measurements indicated a presence of Lepidocrocrite (γ–FeOOH) and Maghemite (γ–Fe_2O_3) on the ITZ. ESEM images showed the existence of microcracks as early as three days after casting with the bridging of these cracks between coarse aggregate locations in the interfacial zone propagating through the mortar. The corroded rebar pullout test results showed a 20–50% reduction in bond strength compared to the corresponding non-corroded rebars. Results of this work could potentially add new dimensions to the existing CRCP construction guidelines related to rebar temperature and surface cleanness at the time of concrete placement, leading to elimination or reduction of horizontal cracking.

4.2 Research objective

The following questions are being investigated in this research:

- What is the effect of rebar temperature at the concrete placement stage on the concrete-rebar bond strength?
- What effect does changing the water-to-cement ratio have on bond strength?
- What effect does using non-corroded rebar steel versus corroded rebar steel have on the concrete-rebar strength and does corrosion play a role in horizontal crack formation?

In this research, water-to-cement ratios of 0.40, 0.45, and 0.50 and their influence on concrete bond strength were investigated. Rebar temperature effects at the concrete placement stage were studied using initial rebar temperatures of 14^{o}F, 77^{o}F, 150^{o}F and 252^{o}F. These temperatures were selected to simulate cold, normal, and hot days when CRCP construction takes place in the field and allowed the investigation of the environmental conditions' effects on rebar concrete bond strength.

4.3 Experimental procedure

Laboratory test specimens were prepared as per ASTM Standard C 192/C 192M-00, "Standard Practice for Making and Curing Concrete Test Specimens in the Laboratory." Cylindrical casts with a diameter of 4 in. x 8 in. length were used for this experiment. The cylindrical casts were made from concrete test cylinder molds conforming to ASTM 470 standard. Fine aggregate gradation was done in accordance to ASTM C 136, "Sieve or Screen Analysis of Fine and Coarse Aggregates." The gradation curve generated from the results showed the fine aggregate type to be dense or well graded, referring to a gradation that is near maximum density. The result obtained from the fineness modulus calculation showed a fineness modulus of 2.7 for the sand used for this experiment; that falls within the expected range for sands used in concrete, which is 2.3 to 3.1. The rebar steel, used for this experiment, was in accordance with ASTM A615, "Standard Specification for Deformed and Plain Billet-Steel Bars for Concrete Reinforcement." The # 6 bar properties used are shown in Table 4.1.

Table 4.1: ASTM A615 requirement

				Deformation Requirements (inches)		
Bar Size	Nominal Weight (lb/ft)	Nominal Diameter (in)	Cross-sectional area ($in.^2$)	Maximum Average Spacing	Minimum Average Height	Maximum Gap
6	1.502	0.75	0.44	0.525	0.038	0.286

The experimental program was designed to evaluate the pullout bond strength. Mixes were designed using ordinary portland cement (OPC) Type I/II, sand, and aggregates. The rebar steel was placed at the center of the cylindrical specimens. The embedment lengths of the rebars were 8 inches. After the specimens were cast, they were covered immediately with a polythene bag to prevent evaporation. The molds were removed after 32 hours of casting and moist cured by spraying with tap water at room temperature until the pullout tests were performed. The pullout tests were conducted at different ages since the bond slip behavior will change depending on concrete strength (bond strength). The testing was done at 3 days, 10 days, and 28 days.

The bond-slip relationship was examined using the pullout test. This was done in accordance with the standard RILEM pullout test, AAC 8.1: "Pullout test for reinforcement." The rebar was gripped by the cross head of an Instron 4482 Tensile tester with a maximum tensile load capacity of 20 kips (88 KN). A specially designed loading frame was fixed to the base of the Instron universal testing machine. The pullout load versus slippage readings were collected electronically and recorded by the computer. A high precision linear variable differential transducer (LVDT) was attached on the loaded end of the steel rebar to measure the displacement from the beginning up to the completion of loading. The average shear stress of the bond based on two measurements was calculated using the maximum shear stress equation used by Abbasi and Hogg, 2005. If the two measured maximum load values were more than 10% different, a third sample was cast and average shear stress was recalculated.

$$\mu_{max} = P_{max} / 2\pi r l_b$$

where P_{max} is the bond force, $2r$ is the diameter, and l_b is the bond length. The pullout rate used was 0.08 in/min with data recorded every one second.

The rebar temperatures were chosen to simulate normal/ambient conditions, hot summer days, and cold winter days, thus simulating rebar temperature conditions during the concrete placement stage. The normal/ambient temperature condition, 77°F, is an approximate room temperature and did not require any adjustment on rebar temperature. Extreme summer temperatures of 150°F and 252°F were achieved by heating the rebar to the desired temperature in a temperature-controlled oven. Rebars were left in the oven for four hours to ensure even heat distribution. A higher-than-normal rebar temperature of 252°F allows study of the effect of extreme heat on concrete-rebar bond failure. Since pavement construction also takes place in extreme winter conditions, a rebar temperature of 14°F was used, and this was achieved by adjusting the thermostat in the refrigerator to 14°F. Rebars were left to cool for four hours to ensure even cooling on the rebar surface. Once the desired temperature was reached, the rebars were removed and immediately inserted in the concrete specimens.

The corrosion of the rebars used for this study was achieved by using an Atlas CCX 3000 Advanced Cyclic Exposure System and the corrosion process done in accordance with ASTM Standard G 85-02, "Standard Practice for Modified Salt Spray (Fog) Testing." Details of the mix proportions and design are reported in reference Sudoi, 2008. An average thickness loss (for 10 sample measurements) was 1.33% of the initial rebar diameter due to the corrosion process.

4.4 Results and discussion

4.4.1 Rebar temperature effects in as-received samples

Laboratory test specimens were prepared as per ASTM Standard C 192/C 192M-00 "Standard Practice for Making and Curing Concrete Test Specimens in the Laboratory." Cylindrical casts with a diameter of 4 in. x 8 in. length were used for this experiment. The cylindrical casts were made from concrete test cylinder molds conforming to ASTM 470 standard. Fine aggregate gradation was done in accordance to ASTM C 136, "Sieve or Screen Analysis of Fine and Coarse Aggregates." The gradation curve generated from the results showed the fine aggregate type to be dense or well graded, referring to a gradation that is near maximum density. The result obtained from the fineness modulus calculation showed a fineness modulus of 2.7 for the sand used for this experiment; that falls within the expected range for sands used in concrete, which is 2.3 to 3.1. The rebar steel used for this experiment was in accordance to ASTM A615, "Standard Specification for Deformed and Plain Billet-Steel Bars for Concrete Reinforcement." The # 6 bar properties used are shown in Table 4.1.

Figure 4.1 shows pullout strength of as-received rebar samples for different water-to-cement ratios at different temperatures after 28 days of concrete setting. The results show a reduction in the peak pullout strength as the temperature increased (Figure 4.1). Similar results were obtained for 10 days exposed samples (not shown). Samarai et al. (1983) showed that the higher the curing temperature, the higher the heat release. The high rebar temperature therefore leads to a rapid buildup of heat on the rebar-concrete interface, resulting in the localized evaporation of water molecules within this region and so a reduction in concrete bond strength. Several research studies have been undertaken to investigate the effect of elevated temperatures exposure in reinforced concrete on the rebar concrete bond strength. Katz et al. (2000) studied the effect of high temperature concrete exposure on the bond strength between fiber reinforced polymers reinforcing bars and concrete. By using a heat jacket around their concrete specimen,

they varied the temperature applied from 68°F to 392°F and performed pullout tests to determine the average bond strength. They found that there was a severe reduction in the bond strength as the temperature rose. Their experiments also showed a high bond strength characteristic and a high pullout peak load at low temperature.

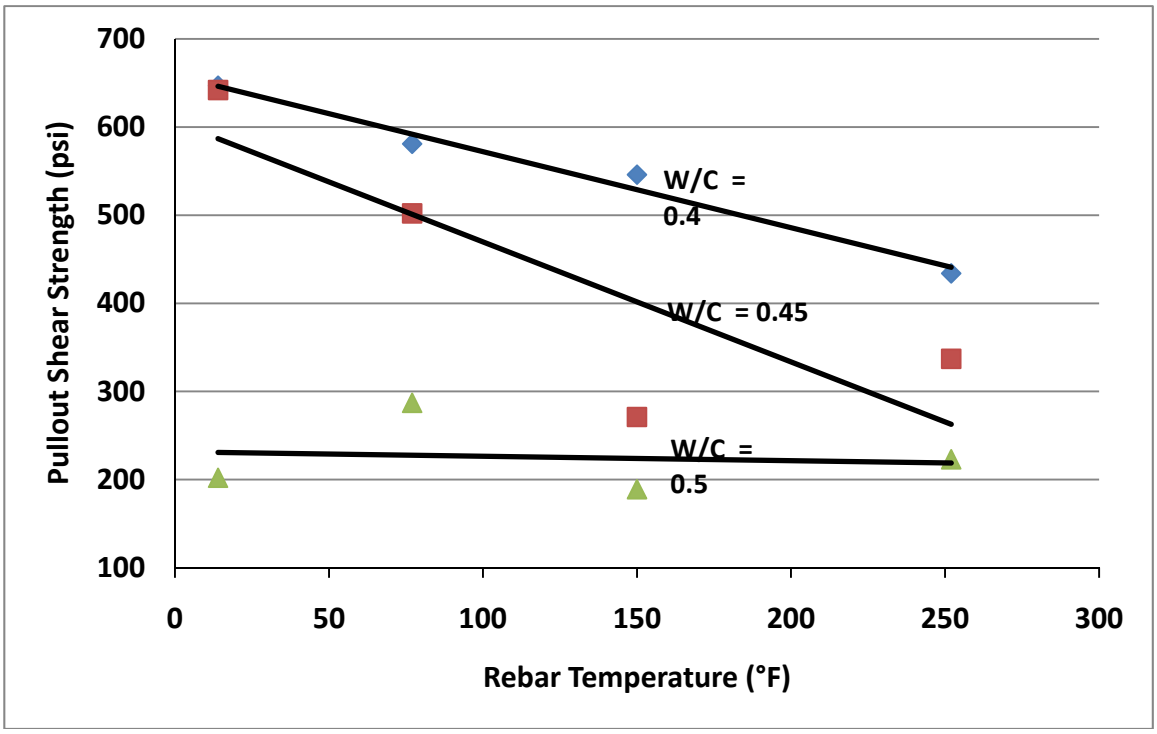

Figure 4.1: Bond strength vs. rebar temperature pullout test results for non-corroded rebar at 28 days

4.4.2 Water-to-cement ratio effects in as-received samples

The bond strength was significantly influenced by the water-to-cement ratio. The 10-day and the 28-day shear stress measurements showed that the lower the water-to-cement ratio, the higher the rebar concrete bond strength (Table 4.2, Figure 4.2). The 28 days pullout tests for 14°F rebar temperature showed a relatively higher bond strength magnitude: 647 psi, 642 psi, and 202 psi compared to the 252°F bond strength magnitudes of 434 psi, 337 psi, and 223 psi for the w/c ratios of 0.40, 0.45, and 0.50 respectively (Figure 4.2). The 77°F rebar temperature bond strength magnitudes at 28 days for the w/c ratios of 0.40, 0.45, and 0.50 were 581 psi, 502 psi, and 287 psi respectively (Table 4.2, Figure 4.2). The high w/c ratio of 0.50 yielded a low bond strength concrete due to the increase in porosity created during the hydration process. The heat of rebars at 252°F evaporated water at the rebar-concrete interface, leading to erratic pullout force data indicated by ** in Table 4.2.

Table 4.2: Measured Bond Strength Magnitudes for non-corroded Rebar Steels at Different w/c Ratios and Rebar Temperatures, 8-in. Embedment

w/c	Temp (^oF)	Pullout Force (lbf)			Shear Stress (psi)			Extension (in)		
		3day	10day	28day	3day	10day	28day	3day	10day	28day
0.40	14	5644	10459	12204	299	554	647	0.140	0.228	0.251
0.45		6457	8303	12102	342	440	642	0.215	0.264	0.253
0.50		6541	8218	3816*	347	436	202	0.330	0.156	0.115
0.40	77	9726	10296	10969	515	546	581	0.344	0.205	0.395
0.45		7402	5884*	9463	392	312	502	0.643	0.209	0.210
0.50		6639	5730	5424	352	303	287	0.935	0.171	0.154
0.40	252	4924	7021	8193	261	372	434	0.144	0.227	0.211
0.45		4879	5475	6357	258	290	337	0.157	0.191	0.224
0.50		5213**	3623**	4208**	276	192	223.	0.204	0.126	0.135

***outliers due to experimental errors**

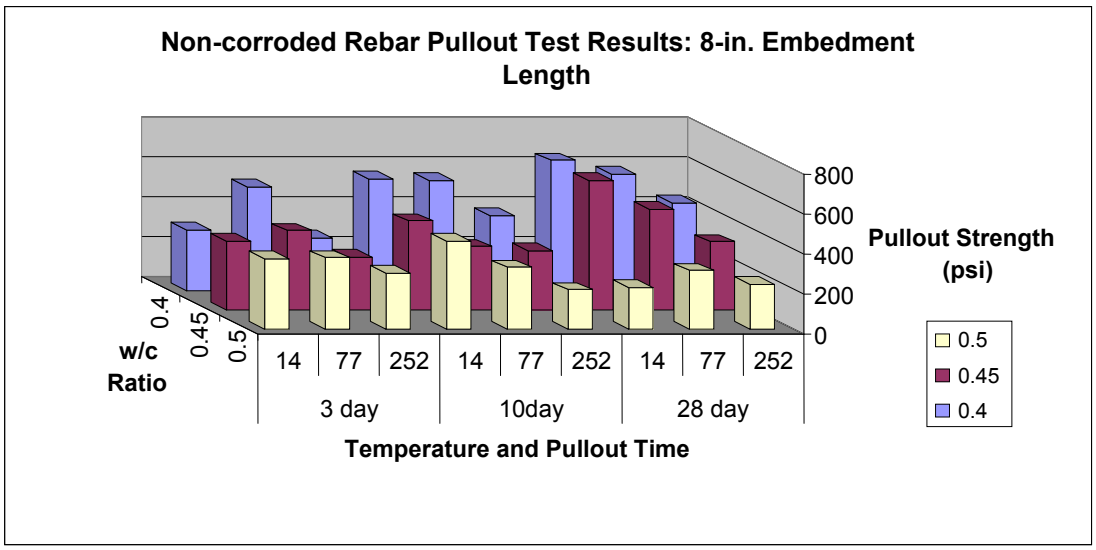

Figure 4.2: Non-corroded rebar pullout test results 8-in. embedment length at different pullout times, temperature and w/c ratios

4.4.3 Rebar temperature effects in corroded samples

The pullout test results on the corroded rebars also showed reduction in the peak pullout strength as the temperature increased, just as observed in the as-received rebars for the 28-day tests (Figure 4.3). The measured bond strength magnitudes for the 28-day tests at 14^oF rebar temperature were 477 psi, 289 psi, and 202 psi for the w/c ratios of 0.40, 0.45, and 0.5 respectively (Table 4.3). These values were relatively higher compared to the 252^oF rebar temperature values of 302 psi, 214 psi, and 168 psi for the 28-day tests. The pullout load and shear strength measurements were, however, lower for the corroded rebar compared to the as-received rebars. The decrease in bond strength can be attributed to the presence of corrosion products on the concrete rebar interface. These results agree with those done by Batis and

Rakanta (2005), who found that pre-oxidized steels exhibited a great reduction in pullout strength with the bond strength between rebar steel and concrete decreasing with increasing weathering on steels.

4.4.4 Water-to-cement ratio effects in corroded samples

The w/c ratio effects exhibited the same characteristics as observed in the previous experiment with as-received rebars. The 28-day shear stress measurements showed that the lower the water-to-cement ratio, the higher the rebar concrete bond strength (Table 4.3, Figure 4.4). The peak pullout strength values for the 77^{o}F rebar temperature were 422 psi, 259 psi, and 195 psi for w/c ratios of 0.40, 0.45, and 0.50 respectively (Table 4.3).The w/c ratio effects in relation to the bond strength characteristics were also examined by Romagnoli et al. (2002). In their experiment, they observed that the steel-mortar bond strength decreased as the water-to-cement ratio increased. They performed their experiment after 1 year of exposing their specimens to different electrolytes. They found that the rebar-mortar bond strength for the specimens stored in tap water was higher than the bond strength for those stored in 3 percent NaCl solution. The corrosive environment created by the NaCl led to low bond strength, analogous to the corroded rebars used in this experiment.

4.4.5 Rebar surface condition effects in corroded samples

The results of the pullout tests on the corroded rebar showed that the 28-day bond strength decreased by a value between 20–50% compared to the results obtained for the as-received rebars. For example, the 28-day pullout test results for the w/c ratio of 0.40 at 14^{o}F rebar temperature for the as-received rebar was 647 psi compared to 477 psi for the corroded rebar for the same parameters (Table 4.3). Bond strength reduction is a result of the corrosion product, rust, residing at the interface between reinforcement and concrete. This degraded the bond between rebar and concrete. These results are in agreement with those done by Congqi et al. (2004), who studied the influence of corrosion on bonds in reinforced concrete.

Table 4.3: Measured Bond Strength Magnitudes for Corroded Rebar Steels at Different w/c Ratios and Rebar Temperatures, 8-in. Embedment

w/c	Temp (^{o}F)	Pullout Force (lbf)			Shear Stress (psi)			Extension (in)		
		3day	10day	28day	3day	10day	28day	3day	10day	28day
0.40	14	6060	9063	8991	321	480	477	0.167	0.243	0.258
0.45		4355	4940	5461	231	262	289	0.157	0.196	0.186
0.50		2331	3797	3824	123	201	202	0.090	0.118	0.249
0.40	77	6001	7973	8738	318	422	463	0.188	0.186	0.240
0.45		4204	4887	5162	223	259	273	0.180	0.184	0.180
0.50		1653	3676	3591	87	195	190	0.073	0.148	0.126
0.40	252	4548	6781	5704	241	359	302	0.130	0.171	0.176
0.45		4440	4185	4052	235	222	214	0.097	0.160	0.191
0.50		1063	1654	3177	56	87	168	0.042	0.073	0.162

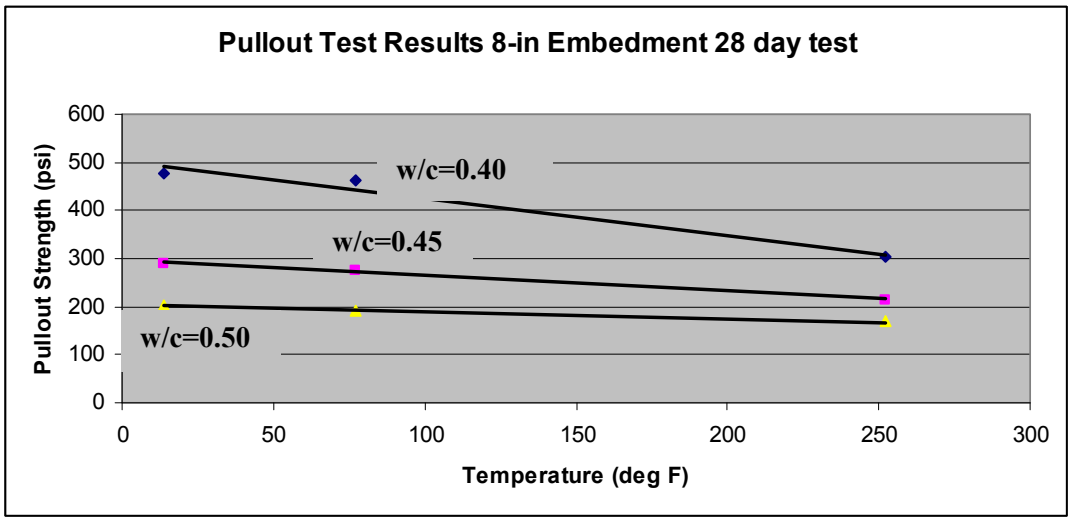

Figure 4.3: Bond strength vs. rebar temperature pullout test results for corroded rebar at 28 days

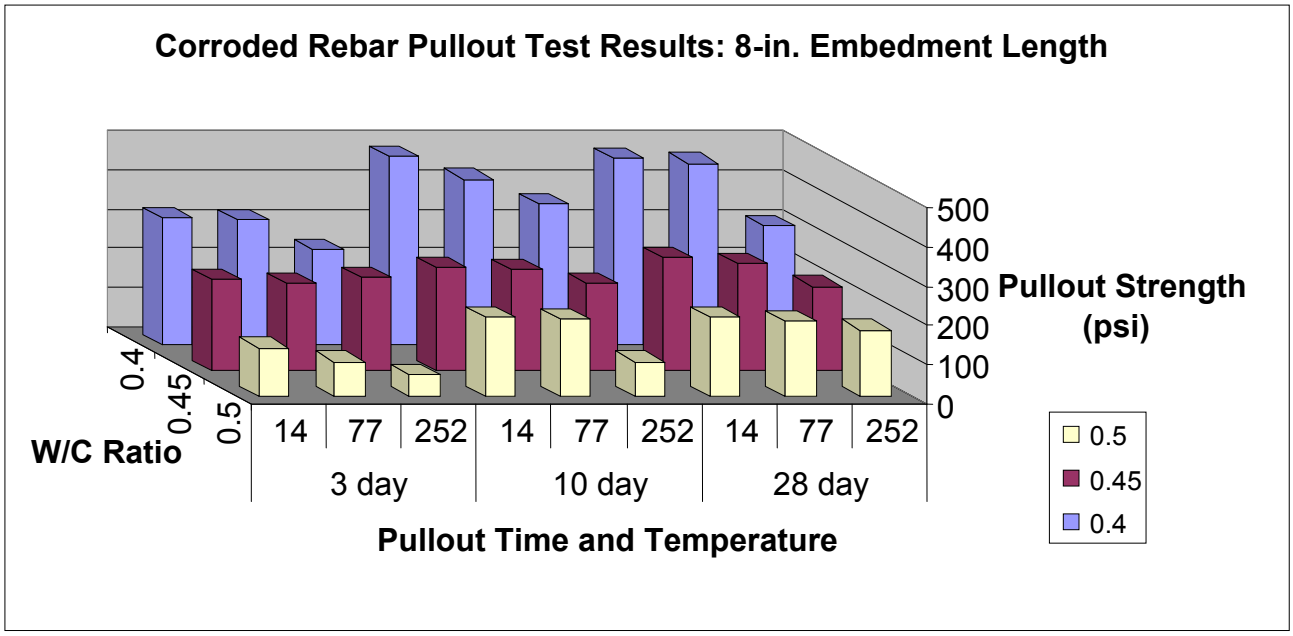

Figure 4.4: Corroded rebar pullout test results 8-in embedment length at different pullout times, temperature and w/c ratios

After mechanical testing, the samples were examined using environmental scanning electron microscopy. An FEI Quanta 200 ESEM was used to examine the interfacial transition zone. Characterization of iron oxides using infrared spectroscopy was performed. In this research, a Nicolet Aviator 370 DTGS FTIR in Attenuated Total Reflection (ATR) mode with Omnic software was used to obtain the infrared spectra in transmittance or absorbance vs. wavelength.

Many investigators have looked into the effects of corrosion on rebar steel-cement bond degradation (10-11, 7). J. L. Gallias (1998) reported that

> "the corrosion layer on the steel combines a physical action before setting and a chemical action during cement hydration. First, high open porosity of the corrosion layer absorbs water of the fresh paste and releases air, creating air bubbles in the limit of the corrosion layer and the cement paste. Second, the steel corrosion products of the outer part of the corrosion layer (iron hydroxides and oxyhydroxides) react with the absorbed calcium hydroxide of the fresh cement paste and produce hexagonal calcium ferrite hydrate."

Cheng et al. (2005) showed that accelerated corrosion after 14 days reduced bond strength by 25.8% for uncoated rebar and 18% for zinc-coated rebar. Batis and Rakanta (2005) compared the results of the pre-rusted rebar samples to those of the clean ones and showed that bond strength was decreased by 22% and 53% when steel rebar samples were exposed to weathering for 45 and 122 days, respectively.

Figure 4.5 shows ESEM micrographs of non-corroded rebar samples kept at 14^{o}F, set after 28 days with water-to-cement ratios of 0.4 (a), 0.45 (b), and 0.5 (c). These images show highly porous and powdery cement formation that did not bond well with the rebar. Figure 4.5 (c) shows crack propagation along the rebar length. SEM images corresponding to room temperature are shown in Figure 4.5 (d, e, and f). The compact cement that formed facilitated better rebar/cement bond formation. Figures 4.5 (e) and (f) show crack bridging between neighboring aggregates. It appears that a region with a dense population of aggregates in the vicinity of the rebar produces a weak link that could potentially become a crack initiation site (Figure 4.5 (e)). Pouring cement on rebar samples kept at 252^{o}F showed the lowest maximum pullout forces (Figure 4.2) compared to room temperature rebar samples. ESEM images corresponding to high temperature rebar samples showed extremely poor rebar/cement bond formation (Figure 4.5 (g-h)). Accumulation of aggregates at the rebar/cement interface (Figure 4.5 (g)), powdery appearance (highly porous cement) (Figure 4.5(h)), and large pore structure (Figure 4.5 (i)) are features seen at the rebar/cement interface of the rebar samples heated to 252^{o}F before concrete placement. These results are indicative of harmful effects of pouring cold concrete on hot reinforcing steels that could potentially develop horizontal cracking on CRCP at the early concrete age.

Figure 4.6 shows ESEM micrographs of corroded rebar samples kept at different temperatures before casting in concrete with various amounts of water-to-cement ratios. The results of the pullout tests on the corroded rebar showed that the 28-day bond strength decreased by values between 20–50% compared to the results obtained from the non-corroded rebar samples. These results agree with results from Batis and Rakanta (2005) in which they found that pre-oxidized steels exhibited a great reduction in pullout strength with the bond strength between rebar steel and concrete decreasing with increasing weathering on steels. Bond strength reduction appears to be the result of the corrosion product, rust, residing at the interface between reinforcement and concrete, and degrading the bond between rebar and concrete. These results are also in agreement with those obtained by Congqi et al. (2004) in their study of the influence of corrosion on bond in reinforced concrete.

The fundamental difference between the corroded and non-corroded rebar tests is the conglomeration of corrosion products on the rebar concrete interface (Figure 4.6 (a)–(i)). The images show a distinct and clear plastering of the corrosion product on the interfacial zone

shown as bright layers on the ESEM pictures, compared to the darker and denser concrete matrix. Energy dispersive x-ray spectroscopy (EDS) was used to chemically characterize the elements on the ITZ and confirm the chemical contents of both light and dark phases. The corrosion products were established to be Maghemite (γ-Fe2O3), Goethite (α-FeOOH), and Lepidocrocite (γ-FeOOH) by FTIR measurements. Maghemite was found to be the dominant phase in the inner layer of rust whereas powdery Goethite or Lepidocrocite forms at the outer layer of the rust. The presence of corrosion products led to the reduction in the pullout peak loads as shown by the pullout tests results given in Table 4.3 and Figure 4.6. These corrosion products prevented the proper development of bond between the rebar and concrete matrix. The ESEM image for the 28-day test specimens for the w/c ratios of 0.50 at 252°F shows a porous structure (Figure 4.6 (i)) similar to what was observed on the non-corroded specimen (Figure 4.5 (i)).

The w/c ratio effects in relation to the bond strength characteristics were also examined by Romagnoli et al. (2002).

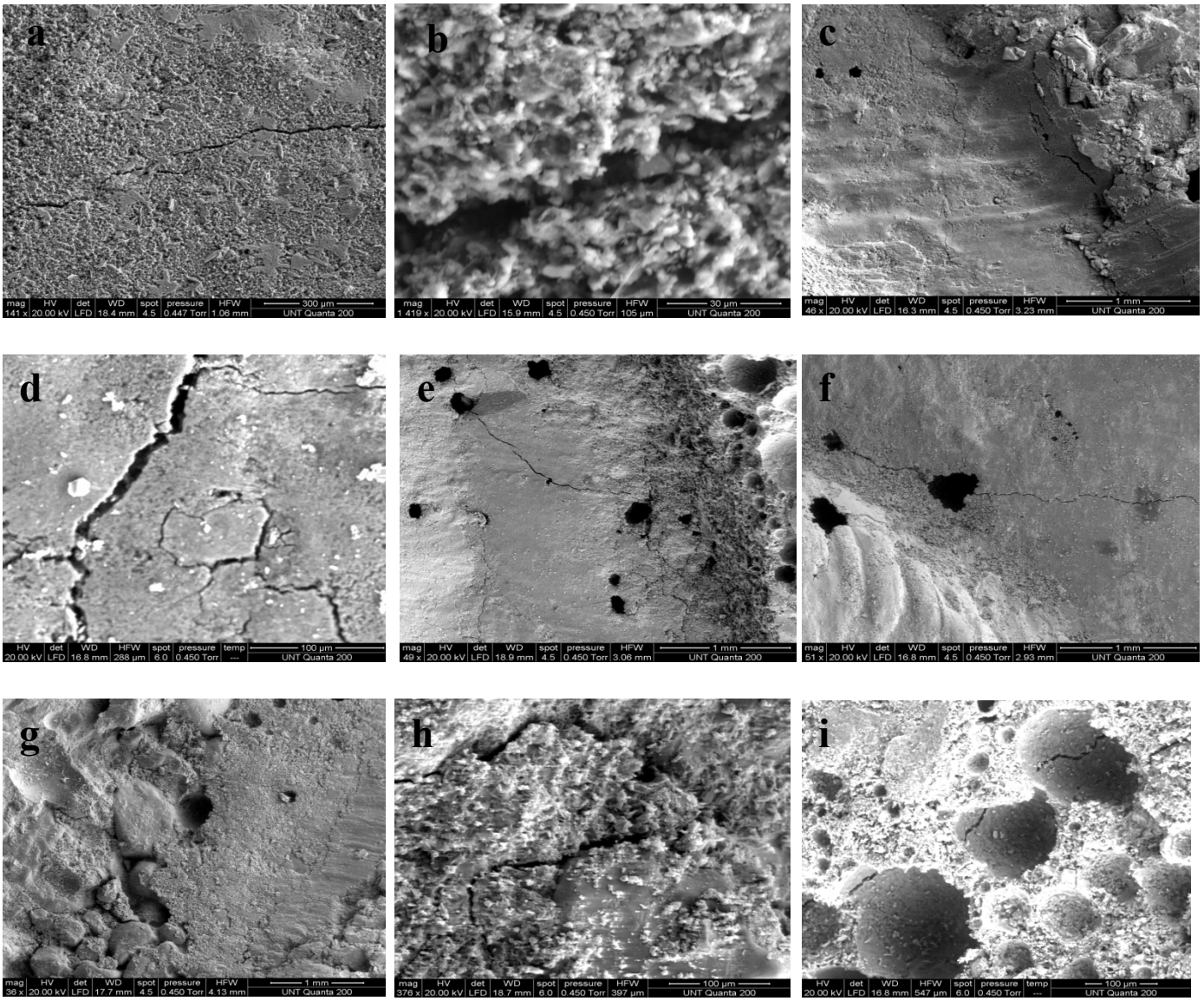

Figure 4.5: ESEM micrographs of the ITZ for non-corroded rebar samples formed at 14°F for w/c 0.40
(a) 14°F for w/c 0.45; (b) 14°F for w/c 0.50; (c) 77°F for w/c 0.40; (d) 77°F for w/c 0.45; (e) 77°F for w/c 0.50; (f) 252°F for w/c 0.40; (g) 252°F for w/c 0.45; (h) 252°F for w/c 0.50; (i) set for 28 days after pullout test

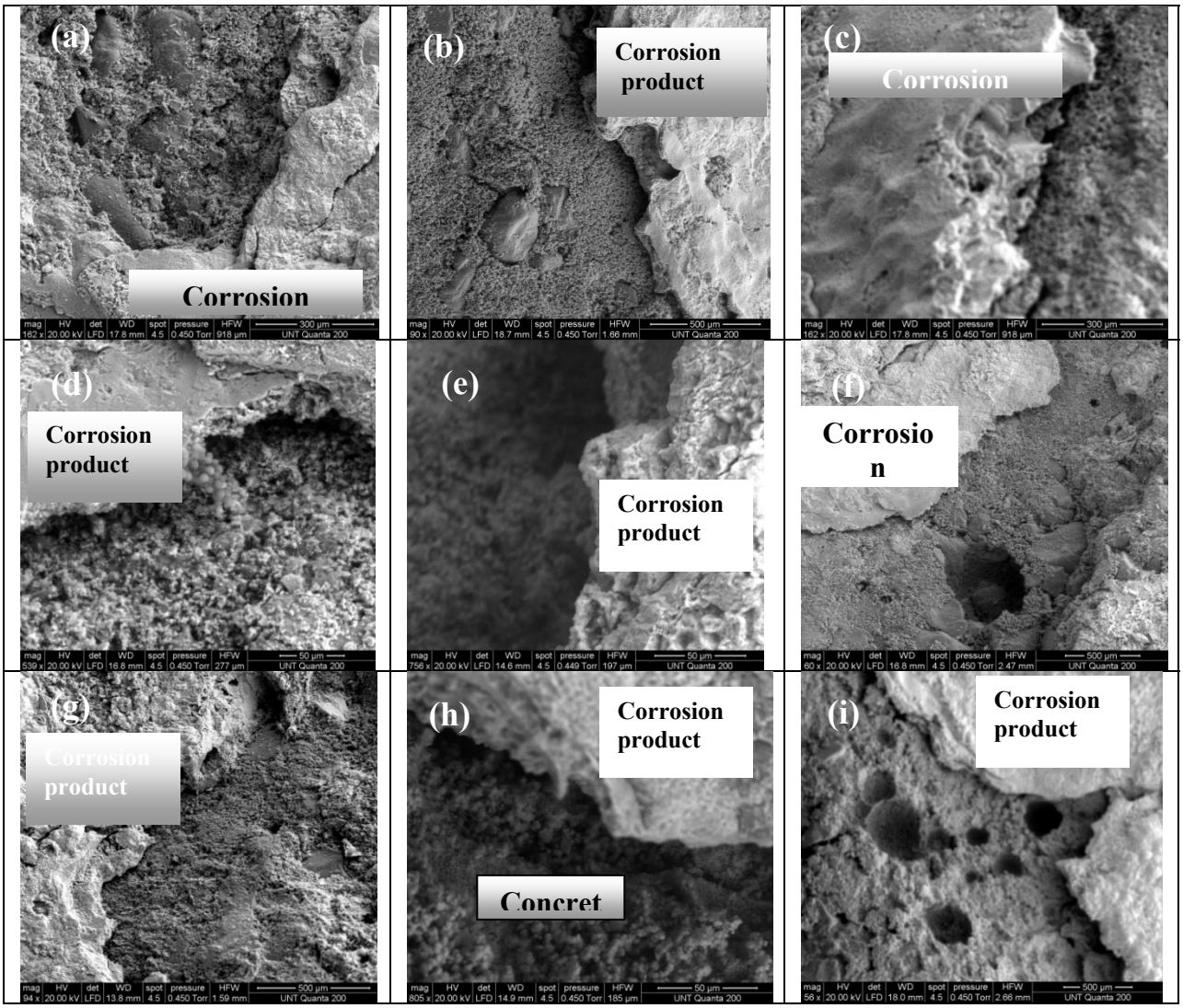

Figure 4.6: ESEM micrographs of the ITZ for corroded rebar samples formed at 14°F for w/c 0.40
(a) 14 ◦F for w/c 0.45; (b) 14°F for w/c 0.50; (c) 77°F for w/c 0.40; (d) 77°F for w/c 0.45; (e) 77°F for w/c0.50; (f) 252°F for w/c 0.40; (g) 252°F for w/c 0.45; (h) 252°F for w/c 0.50; (i) set for 28 days after pullout test

Chapter 5. Conclusions

5.1 Identification of horizontal cracking mechanism

The purpose of this study is to identify the mechanism of horizontal cracking in CRCP. To this end, a numerical model developed to predict the risk of horizontal cracking in CRCP was. Material properties and steel design were considered in the numerical analysis and their effects on the risk of horizontal cracking were investigated. Based on numerical analysis results, laboratory testing was also conducted so that the mechanism of horizontal cracking can be identified. A horizontal cracking frame was developed, in which horizontal cracking was simulated with transverse cracking in a concrete specimen. The mechanism of horizontal cracking was experimentally measured. Based on the findings in this research, the following conclusions are made.

1. Longitudinal steel plays a significant role in the development of horizontal cracks in CRCP. Concrete volume changes due to the variations of temperature and moisture are restrained by the steel at the transverse crack interface and this restraint results in concrete stress. Significant stress of concrete develops near longitudinal steel because of steel restraint. The direction of maximum stress in concrete near steel is almost vertical. It indicates that the horizontal crack perpendicular to maximum stress can occur near the steel. The cracks initiate from the transverse crack interface and propagate along the longitudinal steel.
2. Because horizontal cracks result from restraining concrete volume changes near steel, concrete with a higher CTE will be more likely to induce horizontal cracks in CRCP. A higher elastic modulus of concrete also increases the risk of horizontal cracking. Numerical analysis results imply that the bond-slip condition of steel and the depth of the transverse crack affect significantly the development of concrete stress. Two-mat placement of longitudinal steel may relieve the risk of horizontal cracking in CRCP.
3. A horizontal cracking frame simulated the transverse and horizontal cracks in the concrete specimen with longitudinal steel. During the cooling period, longitudinal and vertical strain suddenly increased. It is considered that these sudden increases were caused by the transverse and horizontal cracks. Test results show an agreement with numerical analysis results. The risk of horizontal cracking increases as the CTE and elastic modulus of concrete become higher.

It is desirable to investigate the accuracy and correctness of the findings from this study through field experimentation.

5.2 Effect of water-to-cement ratio and rebar temperature on bond strength of concrete rebar

The primary objective of this study was to identify the effect of (1) rebar temperature at the concrete placement and (2) the water-to-cement ratio on the concrete rebar bond strength, using as-received rebar versus corroded rebar steel samples. As the result of this research the following conclusions can be made:

1. The rebar-concrete bond strength was significantly influenced by the water-to-cement ratio for both corroded and as-received rebar at all temperatures. The 28-day shear strength measurements showed that the water-to-cement ratio of 0.4 resulted in the highest rebar concrete bond strength. Data presented suggests that the presence of corrosion products adversely affects bonding strength between rebar steel and concrete. Obviously, the weakest link in the CRCP pavement will be the corroded rebar-concrete interface and therefore it is strongly recommended to remove corrosion products from rebar surface before concrete placement.
2. Based on the 10 days and 28 days data (Tables 4.2 and 4.3, Figures 4.2 and 4.4), there was a reduction in the pullout strength as the rebar temperature increased from 14° F to 252° F for both the corroded and as-received rebar experiments. A great deal of attention is directed towards the concrete temperature at the concrete placement stage. To the best of author's knowledge, no mention of the damaging effects of high rebar temperature on bonding is made in the literature. The findings in this research bring this issue in focus. Results of this research highlights the importance of rebar temperature and its adverse consequences on bond strength and authors strongly recommends more in depth analysis of this issue and establishing guidelines that set an upper limit rebar temperature above which placement of concrete is not allowed. Research on understanding the operative mechanism of the interactions of hot rebar surface with cold concrete is currently underway.

Based on the results obtained in this research, it is highly recommended to remove corrosion products from rebar surface before concrete placement. Concrete placement should ideally be done at temperatures close to ambient temperature with a water-to-cement ratio of 0.4.

References

Abbasi A., P. J. Hogg, Temperature and Environmental Effects on Glass Fiber Rebar: Modulus, Strength and Interfacial Bond Strength with Concrete, Composites: Part B Vol. 36 (2005) pp. 394–404.

Batis G., E. Rakanta, Corrosion of Steel Reinforcement Due to Atmospheric Pollution, Cement and Concrete Composites, Vol. 27 (2005) pp. 269–275.

Cheng A., R. Huang, J.K. Wu, and C.H. Chen, Effect of Rebar Coating on Corrosion Resistance and Bond Strength of Reinforced Concrete, Construction and Building Materials, Vol. 19 (2005) 404-412.

Congqi F., K. Lundgren, L. Chen, C. Zhu, Corrosion Influence on Bond in Reinforced Concrete, Cement and Concrete Research, Vol. 34 (2004) 2159–2167.

Gallias J.L., Microstructure of the Interfacial Transition Zone Around Corroded Reinforcement, The Interfacial Transition Zone in Cementation Composites, edited by A. Katz, A. Bentur, M. Alexander, and G. Arliguie, Published in 1998 by E&FN Spon, 11 New Fetter Lane, London EC4P 4EE, UK, ISBN: 0 419 24310 0.

Katz A., N. Berman, Modeling the Effect of High Temperature on the Bond of FRP Reinforcing Bars to Concrete, Cement and Concrete Composites, Vol. 22 (2000) pp.433-443.

Kim S., and Won M., and McCullough B.F., Horizontal Cracking in Continuously Reinforced Concrete Pavements, ACI Structural Journal, V. 101, No. 6, pp. 784-791, 2004

Kim S., Won M., and McCullough B.F., Development of a Finite Element Program for Continuously Reinforced Concrete Pavements, Report 1758-S, Center for Transportation Research, University of Texas at Austin, 1997

Kim S., Won M., and McCullough B.F., Three Dimensional Nonlinear Finite Element Analysis of Continuously Reinforced Concrete Pavements, Report 1831-1, Center for Transportation Research, University of Texas at Austin, 2000

Romagnoli R.O., R. Batik, V.F. Vetere, J.D. Sota, I.T. Lucchini, R.O. Carbonari, The Influence of the Cement Paste Microstructure on Corrosion and the Adherence of Reinforcing Bars as a Function of the Water-Cement Ratio, Anti-Corrosion Methods and Materials, Vol. 49 2002, Issue 1, pp 11-18.

Samarai, M., S. Popovics, and V.M. Malhotra, Effect of High Temperatures on the Properties of Hardened concrete, In Transportation Research Record No. 924, Transportation Research Board of the National Academies, Washington, D.C. 1983, pp 50-56.

Springenschmid R (ed.), Prevention of thermal cracking in concrete at early ages, state of the art report by RILEM TC 119. E&FN Spon, New York, 1998

Sudoi E., Factors Influencing Horizontal Cracking in Continuously Reinforced Concrete Pavements, MS. Thesis, University of North Texas, August 2008.